

Supporting Information

PbTeGeO₆: Polar roesiaite-type germanate featuring two dimensional layered structure

Zhen Jia,^{a,b} Xingxing Jiang,^b Zheshuai Lin^b and Mingjun Xia^{*,b}

^a College of Chemistry and Chemical Engineering, Dezhou University, Dezhou, 253023, China.

^b Beijing Center for Crystal Research and Development, Key Laboratory of Functional Crystals and Laser Technology, Technical Institute of Physics and Chemistry, Chinese Academy of Sciences, Beijing 100190, China.

1. Powder X-ray diffraction: The powder X-ray diffraction (PXRD) data were collected on a Bruker D8 Focus diffractometer equipped with Cu K α radiation ($\lambda = 1.5418 \text{ \AA}$) at room temperature in the 2θ range of $7 - 70^\circ$.

2. Single crystal structure determination: The crystal data were collected by using graphite-monochromated Mo K α radiation ($\lambda = 0.71073 \text{ \AA}$) on a Rigaku Mini single crystal X-ray diffractometer at room temperature. The structure was solved with direct method by program SHELXS-97 and refined by the full matrix least squares on F^2 by SHELXL-97, respectively.¹ During the structural refinement, the Te and Ge atom was refined with the disorder ratio of 0.48:0.52. Therefore, the occupancy ratio of Te/Ge was fixed to 1:1 to make the electroneutral in the structure. All atoms were refined with anisotropic displacement parameters. The crystal structure was verified by the ADDSYM algorithm using program PLATON and no additional symmetry was given.² The crystallographic data and refinement are summarized in Table S1. The atomic coordinates and equivalent displacement parameters are given in Table S2. The selected bond lengths and angles are presented in Table S3.

3. Thermal analysis: The differential scanning calorimetric (DSC) analysis was performed on a LabsysTM TG – DTA16 (SETARAM) thermal analyzer under nitrogen gas flow. The samples was heated from room temperature to $1150 \text{ }^\circ\text{C}$ at a rate of $15 \text{ }^\circ\text{C}$ per minute and then cooled to room temperature at the same rate.

4. UV-VIS-NIR diffuse reflectance spectrum: The diffuse reflectance spectrum was measured on a Varian Cary 5000 spectrophotometer fitted with an integrating sphere in the wavelength range from 200 nm to 1100 nm with BaSO₄ used as a reference material (100% reflectance). The absorption (α/S) spectra were converted from reflectance spectra according to the following Kubelka-Munk function: $\alpha/S = (1-R)^2/2R$, where α , S and R is the absorption, scattering and reflectance coefficient, respectively.³

5. SHG measurement: The SHG measurements of polycrystalline samples were performed with a neodymium doped YAG ($\lambda = 1064 \text{ nm}$) as the incident light source. The SHG signals from samples were detected by a photomultiplier tube. PbTeGeO₆ samples were ground and sieved into five distinct size ranges, 10–30, 30–50, 50–75,

75–105 and 105–150 mm for the test. KDP was served as the reference and sieved into the same size ranges.

6. Computational methods: The first principles calculation was performed to elucidate the relationship between electronic structure and optical properties using CASTEP software package⁴, a plane-wave pseudopotential total energy package based on density functional theory (DFT)^{5,6}. The optimized norm-conserving pseudopotentials⁷ in Kleinman-Bylander form⁸ are employed to model the electron-ion interactions in PbTeGeO₆ and allow the use of a relatively small plane-wave basis set without compromising the accuracy required by this study. The Perdew-Burke-Ernzerhof functionals⁹ in generalized gradient approximation (GGA) form was adopted to describe the exchange and correlation energy. A high kinetic energy cutoff of 800 eV and dense Monkhorst-Pack¹⁰ k-point meshes spanning less than 0.04 Å⁻¹ in the Brillouin zones are chosen. Tests show that these computational parameters give results that are sufficiently accurate for present purposes.

Due to the discontinuous nature of the exchange-correlation functional, the GGA-calculated band gap is smaller than the experimental value. Therefore, scissor operator¹¹ is adopted to raise all the conduction bands to match the calculated band gaps with the measured ones. Based on the scissor-corrected electronic band structure, the imaginary part of the dielectric function can be obtained from the electron transition between the valence band and conduction band, and the real part, i.e., refractive index, can be determined by Kramers-Kronig transform¹². The SHG coefficients was calculated by the program development in our group^{13,14}

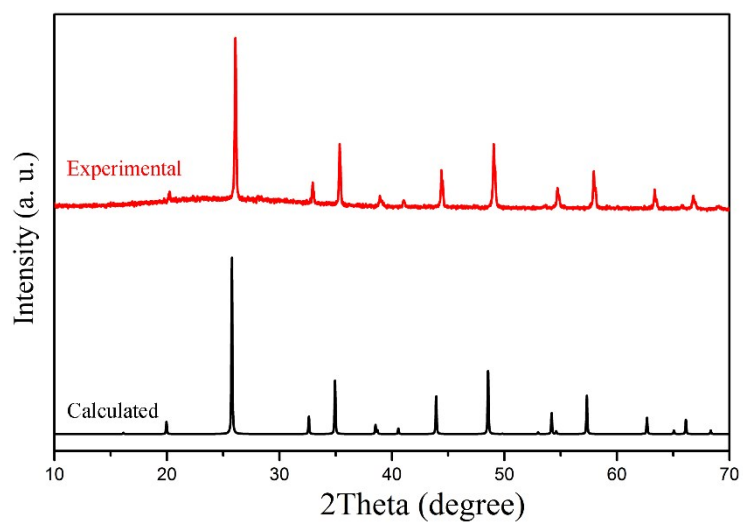


Figure S1. The experimental and calculated powder XRD patterns for PbTeGeO_6 .

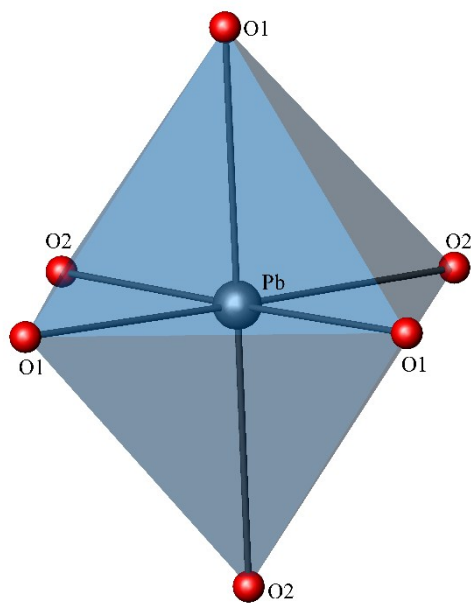


Figure S2. The coordination environment of distorted PbO_6 octahedron.

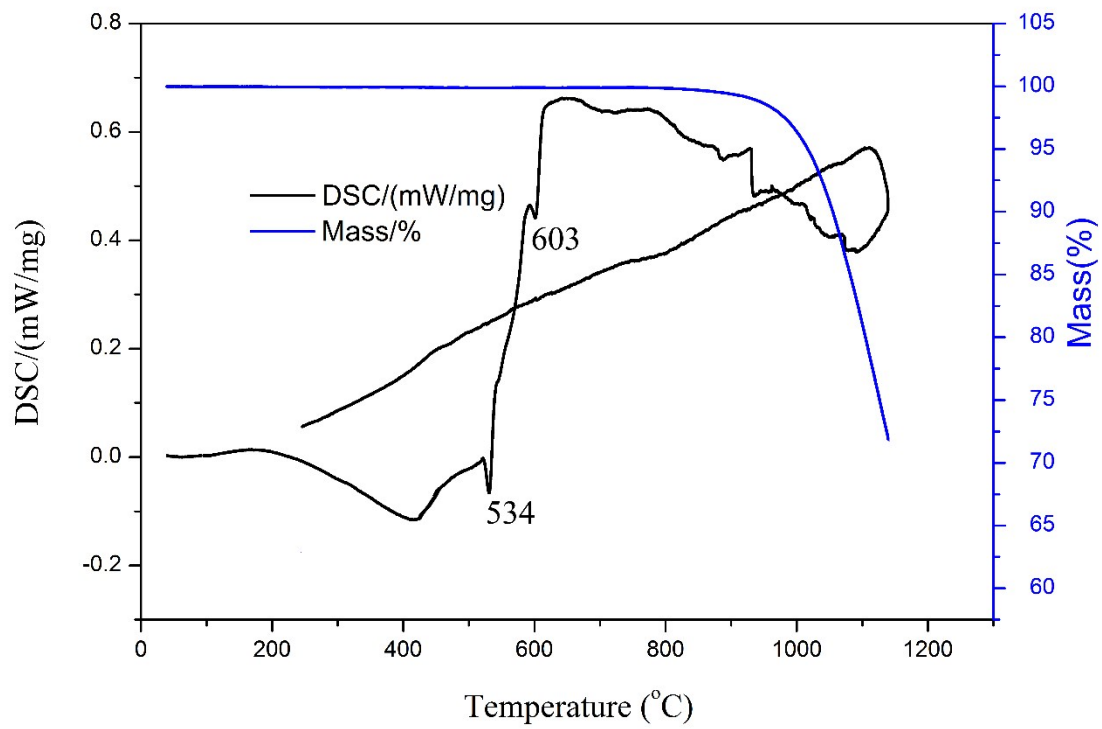


Figure S3. The DSC and TG curves of PbTeGeO_6 .

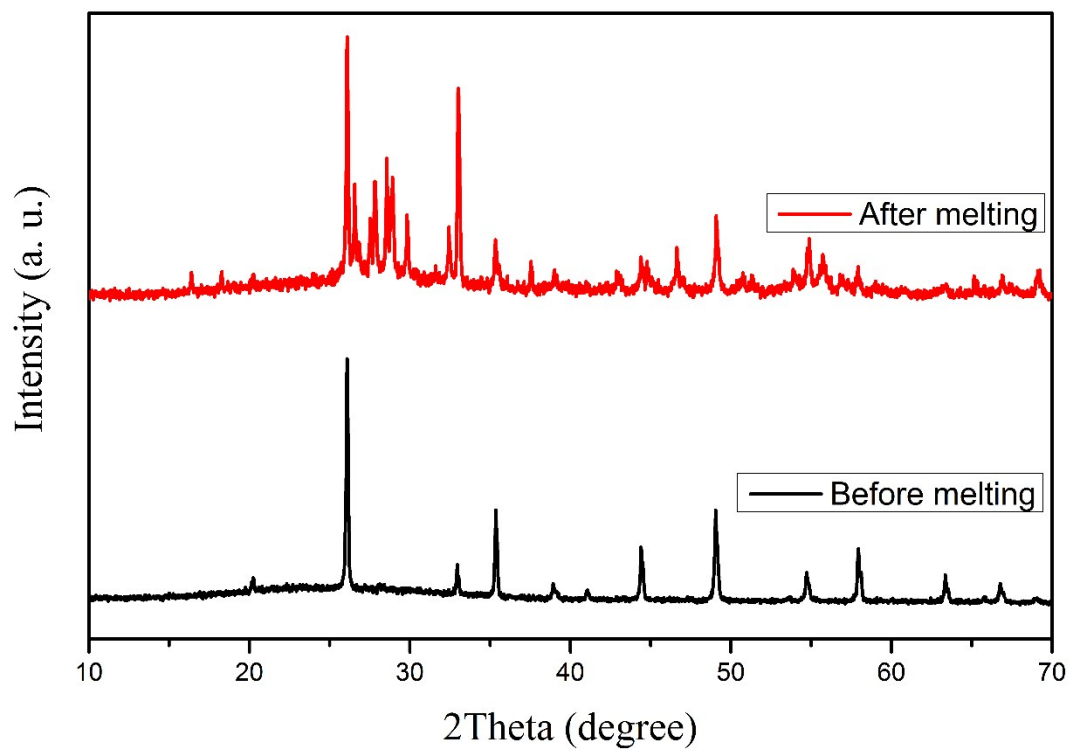


Figure S4. The XRD patterns of PbTeGeO₆ before and after melting.

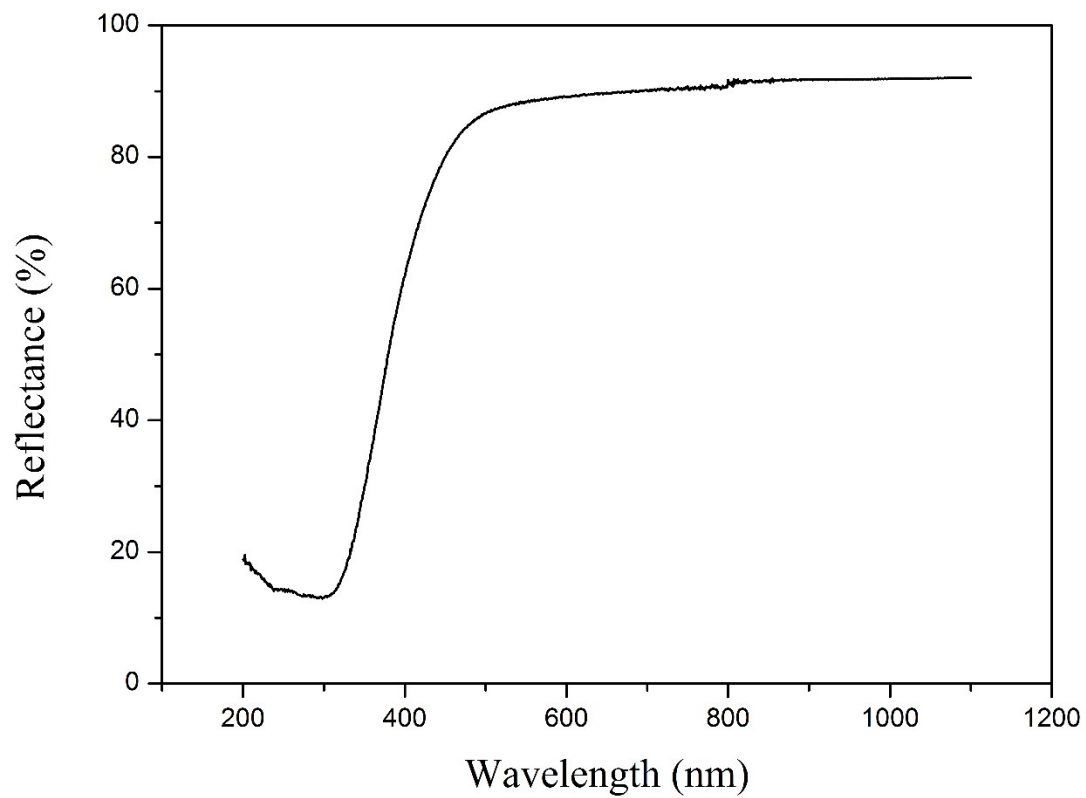


Figure S5. The UV-vis-IR reflectance spectra of PbTeGeO₆.

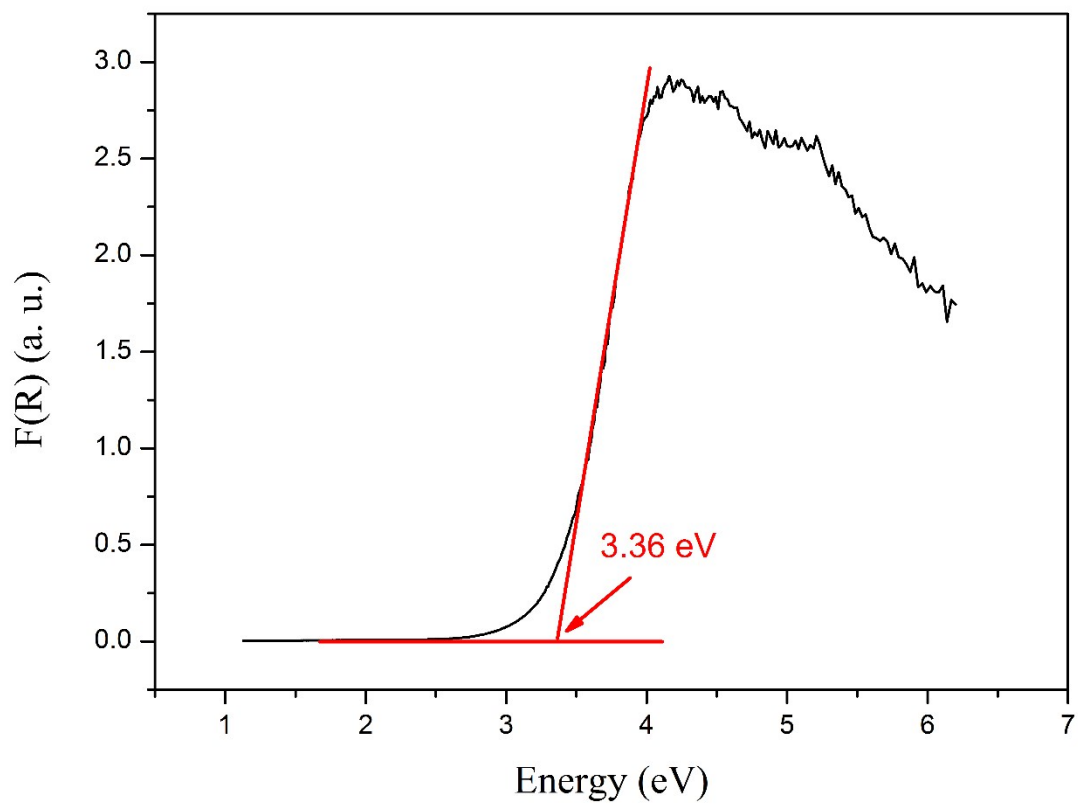


Figure S6. The band gap spectra of PbTeGeO₆.

Table S1. Crystal data and structure refinement for PbTeGeO₆.

Formula	PbTeGeO ₆
Wavelength (Å)	0.71073
Crystal system	Trigonal
Space group	<i>P</i> 31m (No.157)
a (Å)	5.131(8)
c (Å)	5.486(11)
Z	1
Volume (Å ³)	125.1(4)
Density (g/cm ³)	6.682
Absorption coefficient (mm ⁻¹)	45.275
F(000)	214
Goodness-of-fit on F ²	1.092
Final R indices [I>2σ(I)] ^a	R1 = 0.0244, wR2 = 0.0615
R indices (all data) ^a	R1 = 0.0254, wR2 = 0.0622
${}_aR1 = \frac{\sum F_o - F_c }{\sum F_o }, wR2 = \left\{ \frac{\sum [w(F_o^2 - F_c^2)^2]}{\sum [w(F_o^2)^2]} \right\}^{1/2}$	

Table S2. Atomic coordinates and equivalent isotropic displacement parameters (\AA^2) for PbTeGeO_6 . U_{eq} is defined as one third of the trace of the orthogonalized U_{ij} tensor.

Atom	x	y	z	U_{eq}
Pb	0	0	0.30975(14)	0.0140(6)
Te	1/3	2/3	0.8096(8)	0.0100(6)
Ge	1/3	2/3	0.8096(8)	0.0100(6)
O1	0.374(5)	0.374(5)	0.003(4)	0.017(4)
O2	0	0.385(4)	0.607(4)	0.006(4)

Table S3. Selected bond lengths (Å) for PbTeGeO₆.

Pb-O1 (×3)	2.55(2)	Te/Ge-O1 (×3)	1.933(17)
Pb-O2 (×3)	2.56(2)	Te/Ge-O1 (×3)	1.943(15)

Reference:

- (1) Sheldrick, G. M. *Acta Crystallogr. A* **2008**, *64*, 112.
- (2) Spek, A. L. *J. Appl. Crystallogr.* **2003**, *36*, 7.
- (3) Kubelka, P. Z. *Tech. Phys.* **1931**, *12*, 593
- (4) Clark, S. J.; Segall, M. D.; Pickard, C. J.; Hasnip, P. J.; Probert, M. J.; Refson, K.; Payne, M. C. *Z. Krist.* **2005**, *220*, 567.
- (5) Kohn, W.; Sham, L. J. *Phys. Rev.* **1965**, *140*, 1133.
- (6) Payne, M. C.; Teter, M. P.; Allan, D. C.; Arias, T. A.; Joannopoulos, J. D. *Rev. Mod. Phys.* **1992**, *64*, 1045.
- (7) Perdew, J. P.; Wang, Y. *Phys. Rev. B* **1992**, *46*, 12947.
- (8) Kleinman, L.; Bylander, D. M. *Phys. Rev. Lett.* **1982**, *48*, 1425.
- (9) Perdew, J. P.; Burke, K.; Ernzerhof, M. *Phys. Rev. Lett.* **1996**, *77*, 3865.
- (10) Monkhorst, H. J.; Pack, J. D. *Phys. Rev. B* **1976**, *13*, 5188.
- (11) Godby, R. W.; Schluter, M.; Sham, L. J. *Phys. Rev. B* **1988**, *37*, 10159.
- (12) D, P. E. *Handbook of Optical Constants of Solids*; Academic: New York, 1985.
- (13) Lin, Z.; Jiang, X.; Kang, L.; Gong, P.; Luo, S.; Lee, M.-H. *J. Phys D-Appl. Phys.* **2014**, *47*, 253001.
- (14) Lin, J.; Lee, M. H.; Liu, Z. P.; Chen, C. T.; Pickard, C. J. *Phys. Rev. B* **1999**, *60*, 13380.